PHYSICAL REVIEW B **94**, 155447 (2016)

Formation of the $BiAg_2$ surface alloy on lattice-mismatched interfaces

Z. M. Abd El-Fattah,[1,2,3,*] P. Lutz,[2] I. Piquero-Zulaica,[4] J. Lobo-Checa,[4,5,6] F. Schiller,[4] H. Bentmann,[2] J. E. Ortega,[3,4,7] and F. Reinert[2]

[1]*Physics Department, Faculty of Science, Al-Azhar University, Nasr City, E-11884 Cairo, Egypt*
[2]*Experimentelle Physik VII and Röntgen Research Center for Complex Materials (RCCM), Universität Würzburg, Am Hubland, D-97074 Würzburg, Germany*
[3]*Donostia International Physics Center, Paseo Manuel Lardizabal 4, E-20018 Donostia-San Sebastián, Spain*
[4]*Centro de Física de Materiales, CSIC/UPV-EHU-Materials Physics Center, Manuel Lardizabal 5, E-20018 San Sebastián, Spain*
[5]*Instituto de Ciencia de Materiales de Aragón (ICMA), CSIC-Universidad de Zaragoza, E-50009 Zaragoza, Spain*
[6]*Departamento de Física de la Materia Condensada, Universidad de Zaragoza, E-50009 Zaragoza, Spain*
[7]*Universidad del País Vasco, Departamento de Física Aplicada I, E-20018 San Sebastián, Spain*

(Received 25 July 2016; published 28 October 2016)

We report on the growth of a monolayer-thick $BiAg_2$ surface alloy on thin Ag films grown on Pt(111) and Cu(111). Using low energy electron diffraction (LEED), angle resolved photoemission spectroscopy (ARPES), and scanning tunneling microscopy (STM) we show that the surface structure of the $\frac{1}{3}$ ML Bi/x-ML Ag/Pt(111) system ($x \geqslant 2$) is strongly affected by the annealing temperature required to form the alloy. As judged from the characteristic $(\sqrt{3} \times \sqrt{3})R30^\circ$ LEED pattern, the $BiAg_2$ alloy is partially formed at room temperature. A gentle, gradual increase in the annealing temperatures successively results in the formation of a pure $BiAg_2$ phase, a combination of that phase with a (2×2) superstructure, and finally the pure (2×2) phase, which persists at higher annealing temperatures. These results complement recent work reporting the (2×2) as a predominant phase, and attributing the absence of $BiAg_2$ alloy to the strained Ag/Pt interface. Likewise, we show that the growth of the $BiAg_2$ alloy on similarly lattice-mismatched 1 and 2 ML Ag-Cu(111) interfaces also requires a low annealing temperature, whilst higher temperatures result in $BiAg_2$ clustering and the formation of a $BiCu_2$ alloy. The demonstration that the $BiAg_2$ alloy can be formed on thin Ag films on different substrates presenting a strained interface has the prospect of serving as bases for technologically relevant systems, such as Rashba alloys interfaced with magnetic and semiconductor substrates.

DOI: 10.1103/PhysRevB.94.155447

I. INTRODUCTION

Heavy metal alloys, such as $BiAg_2$, feature spin-orbit split (SOS) surface states, an essential prerequisite for the manipulation of the spin-polarized current in spintronic devices [1]. Widely explored is the control of such SOS surface states through, for example, doping with alkali metals [2], exposure to noble gases [3], or through the formation of ternary alloys where a second heavy element is added [4]. The combined interest in their surface electronic structure and the limited number of substrates where these alloys could form on top have motivated the search for heavy metal alloys in thin films grown onto different substrates [5]. For example, $BiAg_2$ was obtained on Ag thin films grown onto semiconducting Si(111) aiming to bring the system one step closer to future technological applications [6–8]. The Ag film thickness was $\geqslant$10 ML, and hence the bulk character of the Ag film was already established. However, lower thicknesses are required to eliminate the strong metallic bulk contribution and to maximize possible hybridization with the underlying substrate. In Bi-Ag/Au(111) the minimum Ag film thickness that allows a well defined $(\sqrt{3} \times \sqrt{3})R30^\circ$-$BiAg_2$ structure is 2 ML [9]. The attempt to grow $BiAg_2$ on thin Ag films (2–5 ML) on Pt(111) has been reported to form a novel (2×2) superstructure for a significant range of Bi coverages (0.2 ML to 0.6 ML) [10]. The authors attributed the absence of the $(\sqrt{3} \times \sqrt{3})R30^\circ$ phase to the strain at the interface between the Ag film and the Pt substrate, which is almost negligible at the Ag/Au(111) interface. Surprisingly, the $BiAg_2$ alloy did not form on Pt(111) for a 5 ML Ag film although the LEED and ARPES data showed the (1×1) spots and the Shockley surface state at the clean Ag(111) film surface, respectively.

In this work we investigate in details the possible formation of $BiAg_2$ alloy on such lattice-mismatched interface systems. Two different substrates are considered, namely Pt(111) and Cu(111), where the Ag-film/substrate lattice mismatch amounts to ∼4% and ∼12%, respectively. In both cases we observe the formation of the surface alloy as demonstrated by three complementary experimental techniques: low energy electron diffraction (LEED), angle resolved photoemission spectroscopy (ARPES), and scanning tunneling microscopy (STM). The characteristic $(\sqrt{3} \times \sqrt{3})R30^\circ$ superstructure and the Rashba surface state are obtained with different Ag film thickness on both substrates. In fact, the alloy formation takes place at room temperature (300 K), and is constrained to annealing temperatures below (350 ± 20) K. For the Bi-Ag/Pt(111) systems, higher annealing temperatures result in the formation of the previously reported (2×2) superstructure for Ag films with a thickness as high as 100 ML, while the annealed Bi-Ag/Cu(111) shows the formation of $BiCu_2$ alloy at the expenses of the $BiAg_2$ phase. These findings provide a way of growing the $BiAg_2$ alloy and similar Rashba systems on substrates where the mismatch at the film-substrate interface might hinder their formation at reduced films thickness.

*Corresponding author: z.m.abdelfattah@azhar.edu.eg

II. EXPERIMENTAL METHODS

Two ARPES setups have been used: for the Bi/Ag/Pt(111) system, ARPES measurements were performed using a SCIENTA R4000 electron analyzer (Würzburg) equipped with a monochromatized He discharge lamp (MB Scientific) operating at excitation energies of 21.2 eV (He I_α) and 40.8 eV (He II_α). The energy and angular resolution at 21.2 eV were set to ~5 meV and 0.3°, respectively. All measurements were undertaken at 40 K, unless specified. ARPES data on the Bi/Ag/Cu(111) system have been carried out using a SPECS Phoibos 150 electron analyzer (San Sebastián) operating with monochromatized He I_α photons, and with energy and angular resolution of ~15 meV and 0.3°, respectively. These data were collected at 150 K. STM experiments on the Bi/Ag/Cu(111) system were taken at an Omicron VT Setup operating at 300 K. The samples are transferred between ARPES and STM setups without breaking the UHV conditions. Both Pt(111) and Cu(111) substrates were cleaned by successive sputtering-annealing cycles until sharp ARPES bands and (1 × 1) LEED spots are obtained. Ag and Bi are separately evaporated from Knudsen cells with rates of 1 and 0.06 ML/min, respectively. The Ag evaporator was calibrated by depositing 1 ML on a Cu(111) substrate, and annealed to 400 K, until the corresponding gapped surface state is observed [11,12]. Likewise, a $\frac{1}{3}$ ML Bi was calibrated by Bi deposition onto Cu(111) that resulted in a sharp Rashba surface state in ARPES and a *pure* $(\sqrt{3} \times \sqrt{3})R30^\circ$ superstructure in LEED [13,14]. The Ag thin films (x-ML) were first grown onto Pt(111) and Cu(111) held at 300 K and 150 K and subsequently annealed to 600 K and 400 K, respectively. The $\frac{1}{3}$ ML of Bi was then grown on top of the x-ML Ag/Pt(111) and x-ML Ag/Cu(111) systems at 300 K and 150 K, respectively, and later annealed to different temperatures. At each annealing temperature both LEED or STM and ARPES data were acquired. Owing to the surfactant effect of Bi, the data were found to be independent on the deposition order, i.e., equivalent results are obtained when Bi is grown first on both Pt(111) and Cu(111) systems followed by Ag film deposition.

III. GROWTH OF $\frac{1}{3}$ ML Bi ON x-ML Ag/Pt(111)

In Fig. 1 we present LEED patterns for a $\frac{1}{3}$ ML Bi film on ~3 ML Ag/Pt(111). The green circles mark the (1 × 1) spots of Ag/Pt(111) system. After Bi deposition, and without any heat treatment, a clear $BiAg_2$-$(\sqrt{3} \times \sqrt{3})R30^\circ$ is formed [the unit cell is marked by the yellow lines in (a)]. Extra spots, which have been previously assigned to the Bi-$(p \times \sqrt{3})$ structure [15], are also observed. Its unit cell is marked by the white lines. The coexistence of the two phases is frequent for $BiCu_2$ and $BiAg_2$ alloys on Cu(111) and Ag(111), respectively, when the Bi coverage exceeds $\frac{1}{3}$ ML [15,16]. In the present case, it is rather an indication of the partial alloy formation, as the deposition of the equivalent amount on Cu(111), taking the different lattice parameters into account, results in pure $BiCu_2$-$(\sqrt{3} \times \sqrt{3})R30^\circ$ spots. Moreover, the extra spots completely disappear after annealing to ~320 K, leaving a sharp $BiAg_2$-$(\sqrt{3} \times \sqrt{3})R30^\circ$ superstructure, Fig. 1(b). After annealing to ~340 K, a partial dealloying takes place resulting in an additional (2 × 2) superstructure (red lines mark its unit cell),

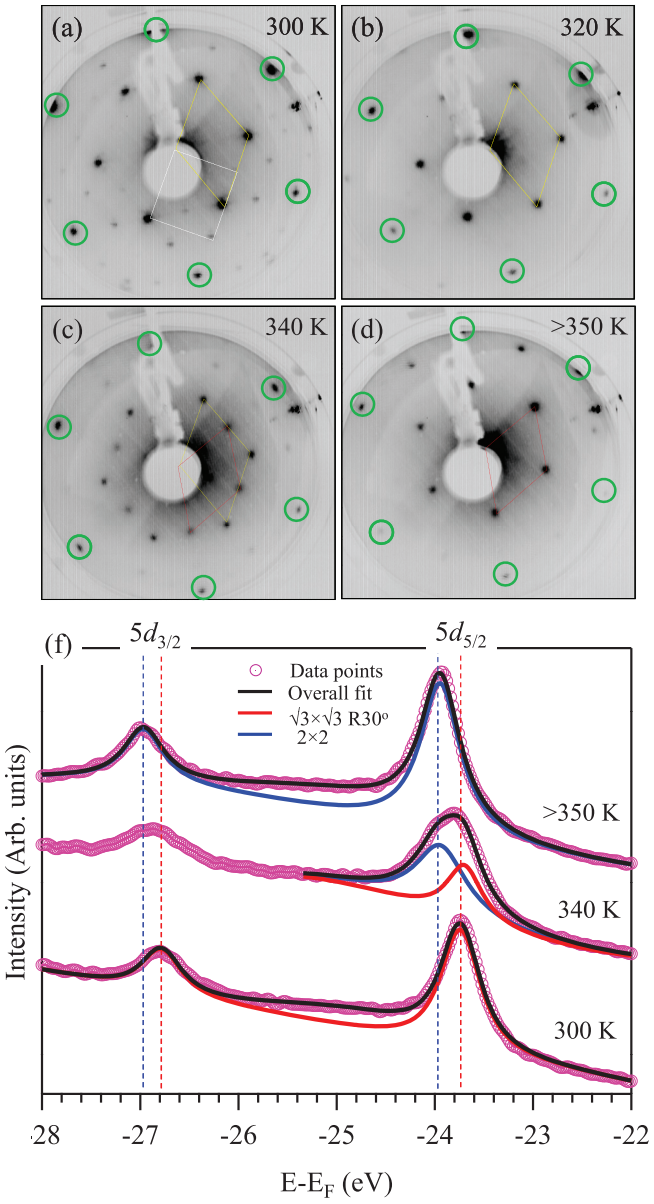

FIG. 1. (a)–(d) LEED patterns for $\frac{1}{3}$ ML Bi grown on 3 ML Ag/Pt(111): (a) as prepared at 300 K, and annealed to (b) 320 K, (c) 340 K, and (d) >350 K. The green circles mark the (1 × 1) spots for Ag/Pt(111). The unit cell of the $(\sqrt{3} \times \sqrt{3})R30^\circ$, the Bi-$(p \times \sqrt{3})$, and the (2 × 2) are, respectively, drawn by yellow, white, and red lines. The electron energy is (45 ± 3) eV. (f) Photoemission spectra of the energy split Bi $5d_{5/2}$ and Bi $5d_{3/2}$ core levels measured with He II_α, for $\frac{1}{3}$ ML Bi-3 ML Ag/Pt(111). The experimental spectra are displayed as purple circles, the overall fitting is denoted by solid black lines, and the red/blue curves are the peak components of the spectra and are, respectively, assigned to the $(\sqrt{3} \times \sqrt{3})R30^\circ$ and the (2 × 2) phases. Data are recorded at 300 K.

Fig. 1(c). At higher annealing temperatures (⩾350 K) a pure (2 × 2) superstructure is obtained, Fig. 1(d). It is important to note that the SOS alloy phase is stable within a very narrow temperature region (<350 K), explaining the absence of this phase in Ref. [10], where the annealing temperature was probably higher. Nonetheless, the strain is likely affecting

the stability of the alloy, considerably reducing the annealing temperature window. We also note that the successive transition from the $(\sqrt{3}\times\sqrt{3})R30^\circ$ + Bi-$(p\times\sqrt{3})$, to the pure $(\sqrt{3}\times\sqrt{3})R30^\circ$, the mixed $(\sqrt{3}\times\sqrt{3})R30^\circ$ and (2×2), and finally the pure (2×2) superstructure is independent on the Ag-film thickness (see Supplemental Material, Fig. S1 [17]) [18–20]. However, the thicker the Ag film becomes, i.e., the lower the overall surface strain, the higher the dealloying temperature becomes.

The $(\sqrt{3}\times\sqrt{3})R30^\circ$-$(2\times2)$ structural transition could be traced by monitoring the Bi $5d$ core level at different annealing temperatures. Figure 1(f) presents these data taken at 300 K with He II_α ($h\nu = 40.8$ eV) for $\frac{1}{3}$ ML of Bi on 3 ML Ag/Pt(111). The experimental and the overall fitting spectra are indicated with purple circles and black solid lines, respectively. The highly asymmetric background is accounted for by a Gaussian edge, made of a pure Gaussian peak on top of a linear background (see Supplemental Material, Fig. S2 [17]). For the as-deposited sample (300 K), we observed a single spin-orbit split peak (red) at binding energies of ~23.74 eV (Bi-$5d_{5/2}$) and ~26.79 eV (Bi-$5d_{3/2}$), i.e., the magnitude of the spin-orbit split amounts to ~3.05 eV. Irrespective of the $(p\times\sqrt{3})$-Bi traces and the Ag film thickness, their energetic positions are always found at (23.70 ± 0.05) eV and (26.75 ± 0.05) eV, being consistent with the reported values for the well-defined $BiAg_2$ alloy on Ag(111) [21]. At 340 K, the intensity of $BiAg_2$ core levels decreases and a new spin-orbit split peak (blue) appears at ~23.95 eV (Bi-$5d_{5/2}$), i.e., ~210 meV shifted towards higher binding energy with respect to the energetic position obtained for the $BiAg_2$ alloy, being now consistent with the reported value for the elemental bismuth [22,23]. This indicates a partial dealloying and the formation of the (2×2) superstructure reported in LEED, Fig. 1(c). At higher annealing ($\geqslant$350 K), the spin-orbit split peak associated with the $BiAg_2$ alloy (red) is completely suppressed, and the overall spectra could be fitted with a single spin-orbit split peak (blue), with its energetic positions at ~23.95 eV (Bi-$5d_{5/2}$) and ~26.97 eV (Bi-$5d_{3/2}$), i.e., corresponding to the (2×2) superstructure. The energetic position of this peak is, within ±50 meV, independent of the Ag film thickness. For all cases studied, beside the characteristic shifts, the magnitude of the spin-orbit splitting is ~30 meV larger for the alloyed phase. The correspondence between LEED and the core-level photoemission data is obvious, and demonstrates the possible formation of the $BiAg_2$ at such strained interface provided that the annealing temperature is reduced. We note that the single $BiAg_2$ phase is hardly obtained given the limited temperature range available; nonetheless, traces of the coexisting phases do not contribute significantly to ARPES spectra [16], as we show next. We also observed that, if the deposition order is reversed, i.e., when Bi is deposited first then Ag on top, the intensity of the Bi $5d$ levels are only weakly affected even for the as-deposited sample (see Supplemental Material, Fig. S3 [17]). This confirms the surfactant nature of Bi, where most of the Bi atoms float to the surface at room temperature [10].

In the following we present ARPES data exclusively for $BiAg_2$ alloy [i.e., after annealing to 320 K (a),(b), 340 K (c), and 400 K (d)] for different Ag film thickness. Figure 2 shows the Rashba SOS surface state obtained for an Ag film thickness as low as 2 ML. Thus a pair of Rashba split bands (red and blue

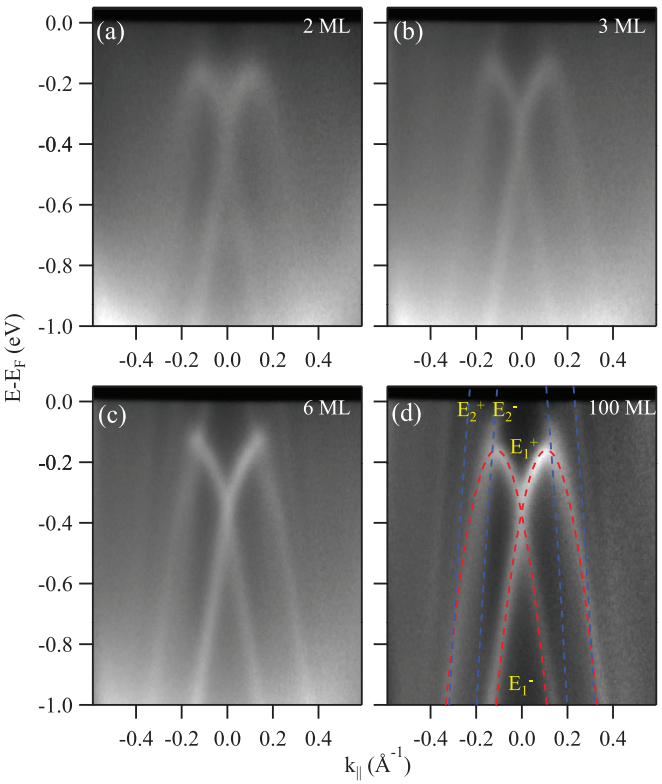

FIG. 2. Surface state band dispersion from $\frac{1}{3}$ ML Bi/x-ML Ag/Pt(111) after annealing to the $BiAg_2$ formation temperatures, where (a) $x = 2$, (b) $x = 3$, (c) $x = 6$, and (d) $x = 100$. The $BiAg_2$ Rashba surface state is seen in all cases with intensity enhancement for thicker films. The blue/red dashed lines assigning the Rashba bands depicted in (d) are obtained from Ref. [9] and indicated in the text.

dashed lines) termed $E_{1,2}$ are observed. Their inner and outer branches are, respectively, denoted by E^- and E^+, as indicated in Fig. 2(d) for the 100 ML Ag film [9]. The major difference is that the quality of the surface states is improved for higher Ag film thickness. Although the Pt(111) substrate is known to significantly alter the dispersion of the surface states of noble metal overlayers for film thickness as high as 4 ML [24,25] due to hybridization with its downward dispersing bulk sp band, the behavior of the Rashba state is practically unaffected indicating its strong localization at the topmost surface layer. The blurred intensity of the surface states for reduced Ag films is likely due to the emission from the underlying bulk Pt band, in addition to the possible roughness of Bi/Ag film [see Fig. 3 on the related case of $BiAg_2$/Ag/Cu(111)].

IV. GROWTH OF $\frac{1}{3}$ ML Bi ON x-ML Ag/Cu(111)

The Ag/Pt system involves a significant interfacial strain so it is interesting to compare it to a system that *a priori* does not have such inherent stress, as is the Ag/Cu(111) interface, which presents a layer-by-layer growth with moiré formation. In Fig. 3 we show STM images taken for $\frac{1}{3}$ ML Bi deposited at 150 K on (a) 1 ML and (b) 2 ML Ag films grown on Cu(111) after gentle annealing to 350 K in both cases. Although the STM images for the 1 ML and 2 ML Ag/Cu

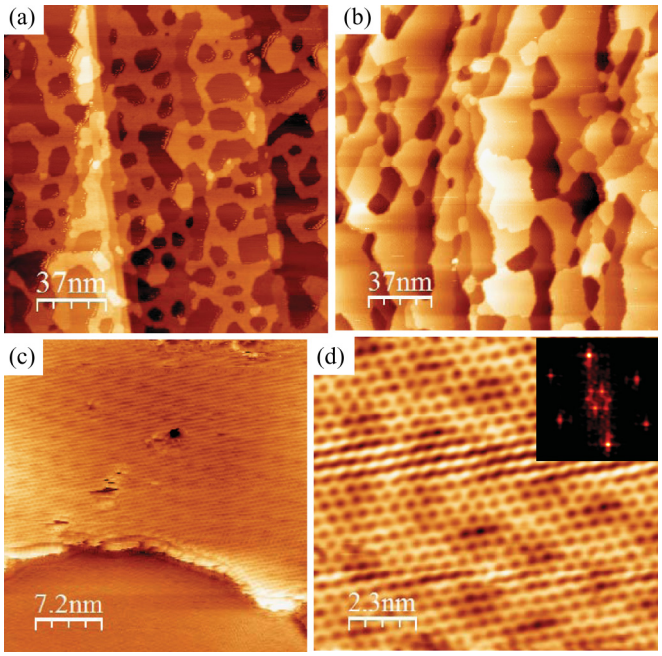

FIG. 3. Large scale STM images for $\frac{1}{3}$ ML Bi grown on (a) 1 ML Ag/Cu(111) and (b) 2 ML Ag/Cu(111), after annealing to (350 ± 20) K. (c) Zoom-in image of (a) revealing a moiré pattern at $BiAg_2$/Ag islands. (d) Atomic scale image of the moiré pattern observed in (c) and its corresponding Fourier transformation of the image in the inset. The latter reveals the atomic structure of the $BiAg_2$ alloy (outer large hexagon) and the moiré pattern (inner small hexagon) and their relative orientation ($\sim 30^\circ$ rotated).

overlayer systems prior to Bi deposition exhibit a perfect layer-by-layer growth (see Supplemental Material, Fig. S4 [17]), the Bi deposition roughens the surface, giving rise to $BiAg_2$/Ag islands (bright areas) and Ag-free areas (dark areas). The $BiAg_2$-covered areas amount to $\sim$50% and $\sim$85% for the 1 ML Ag and 2 ML Ag, respectively, whereas the lateral dimension of the islands is clearly larger for 2 ML Ag. In both cases the height of the majority of the islands is $\sim$4.6 Å, which correspond to bilayer $BiAg_2$/Ag islands. Thicker islands are also observed, which make up for the total 2 ML Ag coverage. On the other hand, excess Bi may begin to alloy with Cu, at apparently structureless Cu areas (see discussion below). A zoom-in image of Fig. 3(a) is shown in Fig. 3(c). The image contains two distinct areas, the Ag-free structureless area and the bilayer $BiAg_2$/Ag region exhibiting a moiré-like pattern. Such a moiré superstructure is characteristic for Bi-free, 2 ML Ag/Cu(111), although the same moiré pattern may also be expected for the $BiAg_2$/Ag/Cu(111) bilayer, as alloying with Bi does not change the Ag-Ag nearest neighbor distance (see Supplemental Material, Fig. S5 [17]). Both the moiré periodicity and the atomic lattice parameter can be deduced from the atomic scale STM image shown in (d). The moiré periodicity is found to be the same as for the 2 ML Ag/Cu (i.e., $\sim$24 Å), whereas the atomic scale resolution reveals the characteristic $BiAg_2$-$(\sqrt{3} \times \sqrt{3})R30^\circ$ with a lattice parameter of 5.1 Å [26]. Furthermore, the moiré pattern is $\sim 30^\circ$-rotated with respect to the atomic lattice, as shown in the Fourier transform at the image's inset.

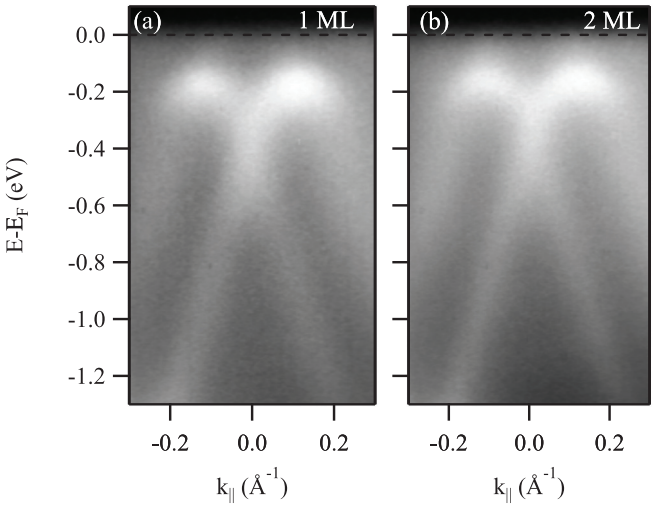

FIG. 4. ARPES photoemission intensity plot after annealing to (350 ± 20) K for $\frac{1}{3}$ ML of Bi on (a) 1 ML and (b) 2 ML Ag/Cu(111). The dispersion relations in both cases are identical, except that the slightly sharper bands in (b) can be associated to the larger lateral extent of the bilayer Ag islands compared to (a).

In Fig. 4 the ARPES photoemission intensity plots for the $\frac{1}{3}$ ML Bi on 1 ML and 2 ML Ag annealed to 350 K are presented. A distinct $BiAg_2$ Rashba surface state is obtained for both Ag coverages. Only a relative improvement in the quality of the surface states is visible, i.e., sharper bands are obtained for the Bi-2 ML Ag sample, as expected for the larger lateral extent of the $BiAg_2$ bilayers in Fig. 3(b). In fact, the quality of the surface states is comparable to the Bi/2-3 ML Ag/Pt(111) presented in Figs. 2(a) and 2(b), indicating that the reduced quality for both systems is related to surface roughness and overall island size. Such a growth behavior is likely triggered by both the well-known high mobility of Ag atoms (kinetics) and the interface mismatch (energetics). The latter is negligible at Ag/Au(111) interface and, therefore, $\frac{1}{3}$ ML Bi on 1 ML Ag/Au(111) exhibits no $BiAg_2$ phase, indicating that a minimum of one Ag bilayer is required for the alloy formation. Another important similarity between the two systems is that the exclusive $BiAg_2$ alloy phase is only obtained at low annealing temperatures (350 K); however, the behavior at higher annealing is very different between both substrates, as we show next.

In Fig. 5 we show ARPES data for a $\frac{1}{3}$ ML Bi grown on 1 ML Ag/Cu(111) at 150 K, and postannealed to (a) 430 K and to (b),(c) 600 K. The $BiCu_2$ surface state can be identified in both cases [3], while the $BiAg_2$ shifts toward higher binding energy. Its Dirac point is now found at (-520 ± 10) meV. It is only at 430 K, where the $BiAg_2$ surface state intensity is comparable to the $BiCu_2$, which can be mistaken with the E_2^- state coming from the unoccupied region. This indicates that the dark areas in Fig. 3(a) are nonalloyed Bi/Cu which transform into $BiCu_2$ alloy upon annealing. The formation of $BiCu_2$ alloy is further justified by measuring its characteristic lattice parameter, $\sim$4.4 Å, in atomically resolved STM images (see Supplemental Material, Fig. S6 [17]). Above this temperature, ARPES data consists mainly of $BiCu_2$ and very weak $BiAg_2$ bands. This mixture of $BiCu_2$ and weak

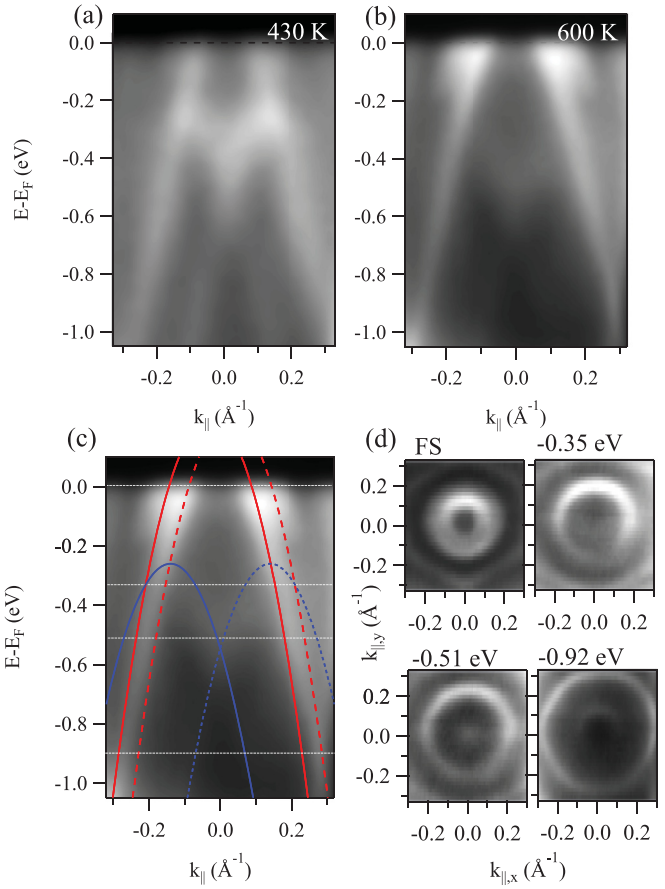

FIG. 5. (a),(b) Photoemission intensity plot for $\frac{1}{3}$ ML Bi on 1 ML Ag/Cu(111) after annealing to (a) 430 K and (b) 600 K. $BiCu_2$ and $BiAg_2$ surface states coexist with the weight of $BiAg_2$ decreasing upon annealing. In both cases the $BiAg_2$ surface state shifts towards higher binding energy compared to the 350 K annealed sample. (c) The same photoemission intensity plot shown in (b) overlaid with the characteristic surface state bands for pure $BiCu_2$ (red lines) and $BiAg_2$ (blue lines). The dispersion parameters are the ones reported for $BiCu_2$/Cu(111) and $BiAg_2$/Ag(111) except that the latter is shifted towards higher binding energy. (d) Constant energy surfaces taken at the indicated energies (white lines) in (c).

$BiAg_2$ surface states is stable up to annealing temperatures of 800 K. The strongly reduced intensity of the $BiAg_2$ surface states clearly indicates a dominant clustering and dealloying at such temperatures. In Fig. 5(c) we overlay the photoemission intensity in (b) with the parabolic dispersion reported for $BiCu_2$ (red lines) and $BiAg_2$ (blue lines) surface states. The red lines coincide with $BiCu_2$ bands, whereas the blue lines are shifted by 110 meV to higher binding energy. The coexistence of the two surface states can also be seen in the constant energy surfaces (CES) taken at the white dashed lines in (c) and presented in (d). The Fermi surface (FS) cut shows the three contours for $BiCu_2$, the -350 meV cut shows the main $BiCu_2$ contour with some inner intensity from the $BiAg_2$, the -510 meV cut shows the main $BiCu_2$ bands and the Dirac point of the $BiAg_2$, and the -920 meV cut shows the $BiCu_2$ (outer) and $BiAg_2$ (inner) rings. The reduced intensity and the shift of the $BiAg_2$ surface state to higher binding energy are likely associated with the presence of two-dimensional $BiAg_2$ crystallites of very small dimensions (see Supplemental Material, Fig. S6 [17]) [27].

V. CONCLUSION

In conclusion, we have shown that it is possible to form the $BiAg_2$ alloy for ultrathin Ag films, even on very strained interfaces. Indeed, the structure of a $\frac{1}{3}$ ML Bi on thin Ag films grown on Pt(111) and Cu(111) is strongly affected by the annealing temperature. For both substrates, the formation of the $BiAg_2$ alloy is only possible for annealing temperatures lower than (350 ± 20) K. The electronic structure of the $BiAg_2$ surface alloy, in both systems, was found to be qualitatively similar to $BiAg_2$/Ag/Au(111). At higher annealing temperatures, the previously reported (2×2) superstructure is obtained on Bi/Ag/Pt(111) independent on the Ag film thickness. However, higher annealing temperatures on Bi/Ag/Cu(111) systems result in the formation of $BiCu_2$ in combination with $BiAg_2$ traces.

The finding that the formation of $BiAg_2$ surface alloy on strained interfaces is limited to a narrow temperature range should have some implications on the search for $BiAg_2$ and similar Rashba alloys on technologically relevant substrates. For example, Ag grows in a layer-by-layer mode on Ni(111), although the lattice mismatch is larger than that for both Cu(111) and Pt(111). Ni(111) supports spin-polarized electronic states and therefore the interplay between Rashba and exchange interactions could be investigated [28,29]. Although the $BiAg_2$ alloy has been previously grown on Si(111) [6–8], the Ag film thickness could be lowered and a Rashba surface state interface with a semiconductor substrate could be obtained.

ACKNOWLEDGMENTS

We would like to acknowledge Dr. Jens Brede for his help during STM data acquisition. This work was supported by the Spanish Gouvernment (Grant No. MAT2013-46593-C6-4-P), the Basque Gouvernment (Grant No. IT621-13), and the Spanish Research Council (Grant No. CSIC-201560I022). Z.M.A. would like to acknowledge funding from DAAD and DIPC. P.L. would also like to acknowledge funding from the Deutsche Forschungsgemeinschaft via Project No.RE 1469/8-1.

[1] C. R. Ast, J. Henk, A. Ernst, L. Moreschini, M. C. Falub, D. Pacilé, P. Bruno, K. Kern, and M. Grioni, Phys. Rev. Lett. **98**, 186807 (2007).
[2] E. Frantzeskakis, A. Crepaldi, S. Pons, K. Kerna, and M. Grioni, J. Electron Spectrosc. Relat. Phenom. **181**, 88 (2010).
[3] H. Bentmann and F. Reinert, New J. Phys. **15**, 115011 (2013).
[4] I. Gierz, F. Meier, J. H. Dil, K. Kern, and Ch. R. Ast, Phys. Rev. B **83**, 195122 (2011).
[5] A. C. Potter and P. A. Lee, Phys. Rev. Lett. **105**, 227003 (2010).
[6] K. He, T. Hirahara, T. Okuda, S. Hasegawa, A. Kakizaki, and I. Matsuda, Phys. Rev. Lett. **101**, 107604 (2008).

[7] E. Frantzeskakis, S. Pons, H. Mirhosseini, J. Henk, C. R. Ast, and M. Grioni, Phys. Rev. Lett. **101**, 196805 (2008).
[8] A. Crepaldi, S. Pons, E. Frantzeskakis, K. Kern, and M. Grioni, Phys. Rev. B **85**, 075411 (2012).
[9] H. Bentmann, S. Abdelouahed, M. Mulazzi, J. Henk, and F. Reinert, Phys. Rev. Lett. **108**, 196801 (2012).
[10] E. Frantzeskakis, S. Pons, A. Crepaldi, H. Brune, K. Kern, and M. Grioni, Phys. Rev. B **84**, 245443 (2011).
[11] F. Schiller, J. Cordón, D. Vyalikh, A. Rubio, and J. E. Ortega, Phys. Rev. Lett. **94**, 016103 (2005).
[12] A. Bendounan, F. Forster, J. Ziroff, F. Schmitt, and F. Reinert, Phys. Rev. B **72**, 075407 (2005).
[13] H. Bentmann, F. Forster, G. Bihlmayer, E. V. Chulkov, L. Moreschini, M. Grioni, and F. Reinert, Europhys. Lett. **87**, 37003 (2009).
[14] L. Moreschini, A. Bendounan, H. Bentmann, M. Assig, K. Kern, F. Reinert, J. Henk, C. R. Ast, and M. Grioni, Phys. Rev. B **80**, 035438 (2009).
[15] K. H. Zhang, I. M. McLeod, M. Lahti, K. Pussi, and V. R. Dhanak, J. Phys.: Condens. Matter **24**, 435502 (2012).
[16] L. Moreschini, A. Bendounan, C. R. Ast, F. Reinert, M. Falub, and M. Grioni, Phys. Rev. B **77**, 115407 (2008).
[17] See Supplemental Material at http://link.aps.org/supplemental/10.1103/PhysRevB.94.155447 for additional information on the Bi/Ag/Pt system at reduced Ag thickness, the fitting of core-level data, the surfactant property of Bismuth, the film roughness induced by Bi deposition, the $BiAg_2$ moiré pattern, and the simultaneous formation of $BiCu_2$ surface alloy and $BiAg_2$ nanocrystallite.
[18] One exception is the ∼2 ML Ag case, where, in addition to the $(\sqrt{3} \times \sqrt{3})R30^\circ$ and the (2×2) spots in Fig. 1(c), traces of the (4×4) superstructure spots were detected. In fact these extra spots could be due Bi/Pt(111) areas present at such a reduced thickness.
[19] M. T. Paffett, C. T. Campbell, and T. N. Taylor, J. Chem. Phys. **85**, 6176 (1986).
[20] Z. M. Abd El-Fattah, P. Lutz, H. Maaß, H. Bentmann, and F. Reinert (unpublished).
[21] H. Bentmann, H. Maaß, T. R. F. Peixoto, C. Seibel, M. Leandersson, T. Balasubramanian, P. Krüger, and F. Reinert, arXiv:1507.04664.
[22] A. V. Naumkin, A. Kraut-Vass, S. W. Gaarenstroom, and C. J. Powell, NIST X-ray Photoelectron Spectroscopy Database (http://srdata.nist.gov/xps/Default.aspx).
[23] M. T. Edmonds, J. T. Hellerstedt, A. Tadich, A. Schenk, K. M. ODonnell, J. Tosado, N. P. Butch, P. Syers, J. Paglione, and M. S. Fuhrer, J. Phys. Chem. C **118**, 20413 (2014).
[24] P. Moras, D. Wortmann, G. Bihlmayer, L. Ferrari, G. Alejandro, P. H. Zhou, D. Topwal, P. M. Sheverdyaeva, S. Blügel, and C. Carbone, Phys. Rev. B **82**, 155427 (2010).
[25] P. Moras, P. M. Sheverdyaeva, C. Carbone, D. Topwal, L. Ferrari, G. Bihlmayer, S. Ouazi, S. Rusponi, A. Lehnert, and H. Brune, J. Phys.: Condens. Matter **24**, 335502 (2012).
[26] C. Kato, Y. Aoki, and H. Hirayama, Phys. Rev. B **82**, 165407 (2010).
[27] G. Vasseur, J. Lobo-Checa, I. Piquero, J. Brede, and J. E. Ortega, (private communication, 2016).
[28] J. Lobo-Checa, T. Okuda, M. Hengsberger, L. Patthey, T. Greber, P. Blaha, and J. Osterwalder, Phys. Rev. B **77**, 075415 (2008).
[29] K. Aït-Mansour and O. Gröning, Surf. Sci. **604**, 872 (2010).